Investigation of Interacting Wake Instability using Complex Network Analysis

Renee Dorer¹ and Jacqueline O'Connor²

Pennsylvania State University, University Park, 16802, USA

Michael Meehan³

University of Colorado – Boulder, Boulder, CO, 80309, USA

The dynamics of interacting wakes is explored using a suite of analytical tools to understand variations in the wake-shedding instability as a function of wake spacing. We use three tools in tandem - wavelet transforms, spectral proper orthogonal decomposition, and complex network analysis – to further investigate the dynamical behavior of a threewake system as compared to a single-wake system. The use of wavelet decompositions allows for a measure of the intermittency in the coherent dynamics of the flow, where the three-wake system displays significantly more intermittency than the single-wake system. The level of intermittency in wake shedding of each individual wake is strongly dependent on the spacing between the wakes, where the dynamics of the central wake are most sensitive to the spacing. Spectral proper orthogonal decomposition and complex network analysis are used together to identify the modal dynamics of the flow as well as the wavemaker regions that drive the oscillations. Analysis shows that the two outer wakes display stronger oscillations than the central wake for most spacings, except where the wakes are strongly merged at the closest spacing. Additionally, the coherence and connectedness of the shear layer oscillations are greater in the three-wake cases, according to the network analysis, as compared to the single-wake configuration.

I. Nomenclature

A = adjacency matrix

C = weighted closeness centrality

D = bluff body diameter

M = number of spatial locations in the flow field N = number of time instances in the velocity data

R = Pearson correlation coefficient R_t = cut-off correlation coefficient

d = least-costly path
i = location index
j = location index
n = time index

= velocity

и

w = bluff-body spacing x = downstream coordinate y = cross-stream coordinate

II. Introduction

Bluff bodies are found in a variety of applications, including boat masts, chimney stacks, and jet engine augmenters [1,2]. In these cases, and many others, the systems are built in multiple bluff-body configurations, rather than a standalone bluff body. Side-by-side bluff-body structures encompass several generic flow features including flow separation, interference between shear layers, vortex impingement, recirculation, and interacting

¹ Graduate Researcher, Mechanical Engineering

² Associate Professor, Mechanical Engineering, AIAA Associate Fellow

³ Post-Doctoral Researcher, Mechanical Engineering

vortex streets [2]. Such features have important implications in engineering design. For example, vortex shedding may result in a large pressure fluctuation on downstream structures as a result of shed vortices impinging on these structures. The resulting pressure fluctuations in turn cause acoustic noise and resonance, the latter of which can result in structural failure [3]. Thus, it is important to understand the phenomenon of multiple-bluff body flows to mitigate the any potential consequences such as structural failure. The goal of this work is to study the dynamics that result from the interaction between the shear layers and wakes of adjacent bluff bodies.

A bluff body flow field consists of three regions. The first is the boundary layer, which is the region of slow-moving flow that develops along the surface of the bluff body. At some point, the boundary layer separates from the bluff body, where the separation point is a function of both the bluff body shape and the velocity of the flow [4–6]. The separation of the boundary layer has two effects: a recirculation zone forms downstream of the bluff body and shear layers (or separated boundary layers) form on either side of the recirculation zone [1,7,8]. Many of the controlling dynamics in these downstream regions of the flow are the result of hydrodynamic instability rather than turbulent motion [9–12]. Bluff-body flows display two main instabilities: the Kelvin-Helmholtz instability and the Benard von Kármán instability. The Kelvin-Helmholtz (KH) instability arises in the shear layers. This convective instability results in the formation of large-scale coherent structures that are associated with the inviscid instability of the mean velocity profile. Meanwhile, the Benard von Kármán (BVK) instability is a global instability in the wake that results in asymmetric vortex shedding [1,7]. The BVK instability is driven by regions of absolute instability, known as "wavemakers," which sustain fluctuations and feed waves into the region downstream of the body [13].

The present study is focused on the coherent instability dynamics of bluff-body flows, which include instabilities in both the shear layer and wake structures of the flow. Several studies on shear layers and wakes used linear stability analysis to understand how disturbances affect the stability of these flows [14-18] Yu et al. [19] used linear stability analysis on a vortex sheet model to study the effects of densities on wakes and jets. The work concluded that absolute instability in these flows is caused by the interaction of two mixing layers. Furthermore, it was concluded that density variation in wakes correlated with the suppression of the von Kármán vortex street, while such variation in the jets lead to self-excited oscillations throughout the entire flow field. Juniper and coworkers used linear stability analysis to study the effects of confinement on jets and wakes [20– 22], revealing that confinement changes the length of any existing recirculation zones, brings shear layers closer to the boundary layer and makes the flow more locally unstable. In addition to analytical methods, experimental studies of the flow around a single bluff body have improved our understanding of the dynamics of wakes and shear layers [5,8,23]. Prasad and Williamson [24] found that, not only is the shear layer instability inherently twodimensional, but that the shear layers also exhibit intermittency. They concluded that a "resonance" observed in the wake in a Reynolds numbers range below that expected shear layer instability was the result of wake-shear layer interaction. Many other studies have shown similar results, as reviewed by Williamson [8]. The dynamics of wake flows have significant impacts on the behavior of flames in reacting systems, where bluff bodies are frequently used for flame stabilization [25]. Work by Emerson and coworkers [26-28] showed the strong connection between the global instability in the wake and the density ratio of the flame.

The dynamics of multi-element flows are fundamentally different than single-element flows, although much of the multi-element flow literature that exists focuses on jets [27,28]. Previous studies of multi-element flows have suggested that the dynamics of the flow field are correlated to the spacing between bluff body centers, w, which are typically normalized by bluff body diameter, D [3]. Many of these studies focus on systems with two bluff bodies. Alam et al. [2], for example, studied the dynamics of the flow behind two side-by-side square cylinders; these results are more thoroughly reviewed by Meehan et al. [29]. Zhou and Alam [3] also provide a summary of the systems used to study bluff body wakes. The time-averaged structure of the multi-wake flow is largely tied to the extent that the recirculation zones behind the bluff bodies can interact. For small spacings (w/D < 1.3), the recirculation zones interact strongly and form a large recirculation zone, even if some fluid is allowed to pass through. For intermediate spacings (1.3 < w/D < 3), a bias exists in the wake structure that is characterized by one large wake and one small wake. It is also in this region that "flip-flopping" behavior is seen, characterized by the gap flow deflecting from one side of the gap flow to another intermittently [30]. Carini et al. [31] studied this behavior using direct numerical simulation and concluded that the flip-flopping behavior is the result of an instability of the in-phase synchronized vortex shedding between the cylinder wakes.

A limited number of studies consider the dynamics of systems with more than two bluff bodies. Sumner et al. [32] studied the flow field for configurations of two and three side-by-side circular cylinders in a flow. Regarding the three-body configuration, Sumner found that small spacings yielded either single bluff body vortex shedding behavior or a biased asymmetric vortex shedding behavior, similar to what was seen in two body flows. For intermediate spacings, the flow experienced biasing like what is seen with two body systems. Interestingly, the biasing in this system was symmetric. Zheng and Alam [33] sought to use direct numerical simulation to classify the behavior of three body flow into regimes in a manner similar to Alam et al. [2]. Sebastian et al. [28] studied the effects of spacing on the dynamics of multi-element flows with both odd and even numbers of wakes using linear stability analysis. The results concluded that the dynamics of the interacting wakes are connected to

the spacing between the bluff bodies as well as the number of bodies in the system. Thus, it is not adequate to draw conclusions about the flow field dynamics of systems with three or more bluff bodies from the findings of dual-bluff body flow studies.

The current study follows previous work on the same three-body configuration used by Meehan et al. [29] and Dare et al. [34]. Meehan et al. [29] explored the intermittency of large-scale coherent structures in three interacting bluff body flows. A proper orthogonal decomposition (POD) was used to decompose the flow field into its highest energy modes. A Hilbert transform identified the relative instantaneous phase between oscillation in each wake and statistical analysis was used to categorized them into different regimes. The study found that the dynamics of the interacting wakes were somewhat predictable for large and small spacings. In fact, they closely mimicked the findings from dual wake literature. Dare et al. [34] clarified the dynamics seen in the data set collected by Meehan et al. with the use of a cluster-based reduced order modeling (CROM) technique. In this methodology, velocity snapshots are organized into groups based on their flow fields using a k-means clustering algorithm. A transition matrix is then determined by calculating the likelihood of transition between each of the states, identifying the most likely transition from one cluster to the next. The study found that there were two main oscillatory patterns in the multi-wake cases, where switching between them was driven by changes in the vortex shedding of the inner shear layers near the recirculation zone. This finding indicates the recirculation zone may be a region that is sensitive to perturbations or changes in the base flow structure.

While the previous work done indicated significant switching behaviors between different oscillation states in multi-wake systems, the tools used did not provide sufficient information about the dynamics of the wake. POD struggles to capture the dynamics of unstable flow fields in their entirety due because relies on spatial correlations only [35]. Therefore, it does not provide any information as to how a flow field will evolve over time or use temporal correlation as a basis for determining mode energy. However, new decomposition methods have been developed to provide further insight. Filtering the flow field using wavelets prior to the use of POD has proven to be successful in detecting dynamics that were not able to be detected using POD alone [36]. Karmarkar et al. [37] used wavelets to filter velocity data from a bluff body stabilized flames prior to decomposing the field in order to identify the impact of turbulence on coherent motions. Another method, spectral proper orthogonal decomposition (SPOD), correlates in both time and space by performing a fast Fourier transform (FFT) on the data prior to decomposition [35].

In addition to SPOD, another method used in this study is complex network theory, which has recently been used to study turbulent flows and combustion instability. Network measures provide more insight into the flow by quantifying the relationship between parameters, such as velocity fluctuations, throughout the flow field. Hashimoto et al. [38] and Kasthuri et al. [39] used measures from complex network theory to study the spatiotemporal dynamics of combustion instability in a model combustor. Both studies were successful in using network measures to characterize the transition to combustion instability in their experimental configurations. Meanwhile, Krishnan et al. [40] used complex network analysis to identify regions that are receptive to disturbances in a bluff-body stabilized combustor with a backward-facing step. They were able to mitigate combustion instability by placing microinjection systems in the regions with high network connectivity. The studies mentioned contribute to the understanding of unstable and turbulent flows by using network measures to quantify how disturbances travel throughout the flow field. In addition, work by Karmarkar et al. [41] used network measures in combination with SPOD to understand the interactions between a global instability and a thermoacoustic instability in swirling flames. These toolsets have the potential to provide more insight into systems with complex, intermittent modal behaviors.

The goal of this work is to study how the source of oscillations in non-reacting multi-wake flows vary with bluff-body spacing by analyzing the data collected in the work of Meehan et al. [29] with a combination of wavelets, SPOD, and complex network analysis. The combination of these tools provides new insight into the intermittency of the oscillations and the regions of the flow that drive the oscillations.

III. Experimental overview

A. Experimental facility

Data were collected in a multiple-wake system previously described by Meehan et al. [29]; a brief overview of the system is provided here. The experiment is shown in Figure 1; it consists of a rectangular duct with two honeycomb flow straighteners and a perforated plate. Three bluff bodies with diameter, D, are located downstream of these flow preparation elements and are attached to tracks, allowing for continual variation of the center-to-center distance between the bluff bodies, w. Each bluff body is a stainless steel, triangular prism; the three sides have equal lengths of 0.75 inches (19.05 mm) and the bluff body has a span of 4 inches (101.6 mm). The bluff bodies are fixed to the experiment with clamps on either end of the span. Near the edge of the experiment, two plates are affixed to the top of the duct to provide a clean outer boundary condition for the flow; initial measurements found high levels of unsteadiness and large-scale vortical entrainment on the edge of the rectangular

duct if these plates were not present. The plates were positioned the same distance away from the outer edge of wakes 1 and 3 (shown in Figure 1a) as in between the inner edges of the bluff bodies.

B. Diagnostics

High-speed PIV is used to obtain axial (x-direction) and transverse (y-direction) velocity data. The laser (Quantronix Hawk-Duo 532 nm Nd:YAG dual cavity laser) outputs light with a wavelength of 532 nm and with a total pulse energy of 10 mJ at 4 kHz, with a pulse width of 190 ns. The beam passes through a collection of sheet-forming optics to form a diverging sheet on top of the experiment. The laser sheet illuminates the aluminum oxide tracer particles, approximately 0.5-2.0 μm in diameter. A Photron FASTCAM© SA5 at full 1024x1024 resolution fitted with a CarlZeiss Makro-Planar® 100 mm lens and 14 mm extension tube records images and velocity data through a 532 nm band pass filter. The resulting spatial resolution is 0.129 mm.

PIV calculations were performed using DaVis 8.3 from LaVision®. For each case, 5001 images are acquired at a data acquisition rate of 4 kHz. The raw seeded images are first preprocessed using a five-frame sliding minimum filter. The vector fields are calculated by using a multi-pass algorithm where the first pass is performed with an interrogation window size of 64x64 and 50% overlap while the final two passes are performed with a 16x16 window size with 50% overlap. This results in a vector resolution of 1.0 mm. Post-processing of vectors in DaVis includes a universal outlier detection scheme with a 3x median filter. This ensures removal of groups with less than 5 vectors and vectors with a residual greater than 2. It also ensures re-insertion of vectors with a residual less than 3. The average number of vectors replaced per dataset range from 5% to less than 7% and the percent first choice vectors are between 88% and 93% for the datasets analyzed in this paper. This processing results in an average PIV uncertainty of approximately 10-15% of the bulk flow velocity and an RMS PIV uncertainty of 9-13% of the bulk flow velocity in the regions of interest for this study.

After the data was acquired, a very small subset of the data just above the top plates and bluff bodies was found to be corrupt. Due to the global nature of the analyses discussed below and the requirement of equal time steps, it was necessary to correct these spurious data points. To do so, a short time series was extracted for each spatial location and feed through a simple outlier detection algorithm based on the root-mean-square (RMS) of the velocity magnitude. The RMS provides a robust means for outlier detection for this situation because the corrupt data appears as extraordinarily large relative velocity magnitude; generally, the velocity magnitude in these regions should be $|u| \le 0.5$ m/s, but the spurious data points were $|u| \ge 5$ m/s. Once identified, one-dimensional cubic spline interpolation using the three previous and three following instances in time was performed to replace the existing corrupt data.

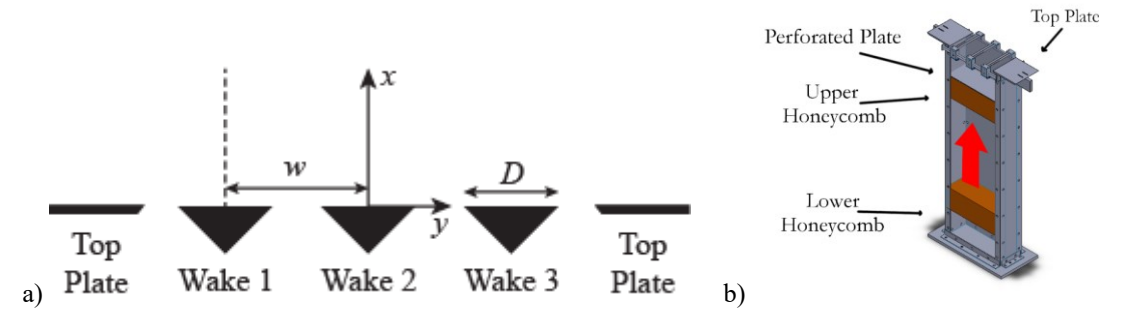


Figure 1. Schematic (a) and drawing (b) of experimental configuration (front plate removed to show flow conditioning).

C. Data analysis

Time domain analysis was first used to quantify the intermittency in the coherent wake dynamics. Following the work of Karmarkar et al. [37], we used wavelet transforms to quantify the coherent velocity oscillations in a variety of locations throughout the flow field. To apply these transforms, a 5x5 interrogation window was selected in a region of high velocity oscillation amplitude that was identified from the SPOD modes, discussed next. The velocity signal over this area was then averaged spatially to prevent spurious results from the use of data from just one interrogation window. From there, the wavelet transform is performed using the *cwt* function in MATLAB® with the 'bump' wavelet option. To quantify intermittency, we calculate an intermittency factor (*IF*) following the methodology of Karmarkar et al. [41] and Prasad and Williamson [24]. First, we used the wavelet transform to identify the appropriate frequency range for analysis; in a wake-shedding situation, we expect these oscillations to be at Strouhal numbers near St = 0.2-0.3. The signal used for the analysis is chosen from this frequency band. Second, we choose a threshold value for the signal. Values that exceeded this threshold are considered coherent in time, as represented by τ_c . This coherent time is then divided by the total time of the signal, or

$$IF = \frac{\tau_c}{T} \tag{1}$$

where *T* is the total time of the signal in seconds.

Two sensitivity studies were performed on the single wake case to understand the effects of frequency band size and threshold on the calculation of the intermittency factor. The results are displayed in Figure 2. In Figure 2(a), a bandwidth of varying width is chosen around the peak frequency of 47 Hz. The trend in *IF* values is non-monotonic with bandwidth and is dependent on the behavior of the frequency spectra. As we increase the range of frequencies, more coherent and incoherent oscillations are captured, resulting in a non-monotonic trend that depends highly on the data set in question. Based on this analysis, the frequency ranges selected for each case in this data set are presented in Table 1. These were chosen to capture the most coherent behavior around the center frequency without capturing too much noise.

Next, the sensitivity of the IF to the threshold value above which the signal is determined to be coherent is plotted in Figure 2(b) as a function of downstream distance. The points in space where the IF was calculated correspond to regions of high coherent oscillation from the SPOD results, discussed later. The results show that the magnitude of the IF is dependent on the threshold value, but that the trend in IF with downstream distance is consistent for a large range of thresholds. For example, setting the threshold to 20% of the peak signal value implies that most of the signal is coherent and leads to intermittency factor values close to 1 for all downstream distances. At the other extreme, considering 80% of the signal to be incoherent removes coherent time from the data. As a result, the intermittency factor is very low throughout the plot and even decreases for x/D values greater than 4.5 rather than approaching an asymptotic value. Trends in IF with downstream distance are similar for threshold values of 40%-70%, and so we select a value of 50% of the peak signal value for analysis in this paper.

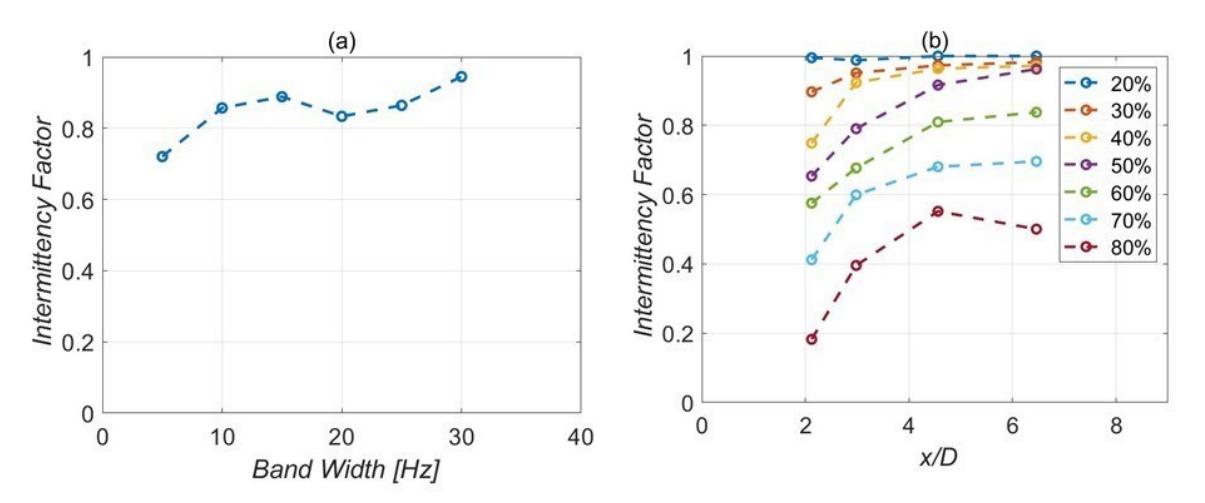


Figure 2. Trends in intermittency factor of the single wake with a) bandwidth of the wavelet filter and b) threshold of the intermittency factor calculation.

w/D	Frequency Band (Hz)
1.68	12-42
1.94	33-64
2.20	43-70
2.47	36-90
2.73	36-55
2.99	35-48

Table 1. Frequency bands selected for calculation of IF at all wake spacings.

Spectral proper orthogonal decomposition, following Towne et al. [30], is used to identify the spectrally coherent oscillations in the flow field. SPOD is an extension of proper orthogonal decomposition (POD) [31], a data-driven modal decomposition that yields energy-ordered modes that can be used to extract coherent structures from a flow field. SPOD builds on this foundation by applying POD to flow snapshots determined at a given frequency by dividing the time-series data into ensembles and applying a Fourier transform. The resultant calculation provides the eigenvalue spectrum of the cross-spectral density between flow oscillations in space at a given frequency rather than the full-time correlation. This process yields optimal spatial modes analogous to those from snapshot POD but that are also frequency-resolved and can therefore be interpreted as representative of coherent flow oscillations at the oscillation frequency considered.

To complement the results from SPOD, we also apply a complex network analysis to identify wavemaker regions of the flow. Wavemakers are regions in the flow that nonlinearly feedback flow oscillations, resulting in

a region of self-excited oscillatory driving [32]. Wavemakers can be readily identified through structural stability analysis [33], but this is often difficult in highly complex flow fields. It is also sometimes difficult to conduct this analysis from experimental data, as the inflow conditions to the flow field, in this case the region upstream of the bluff body, may be important for capturing the dynamics of the flow yet are not typically measured in an experiment. As such, this complex network analysis provides similar insight in realistic experimental data without the drawbacks of using analytical tools on incomplete datasets.

The current method follows that of Krishnan et al. [34], who applied complex network analysis to identify shear layer instability in flow around an axisymmetric bluff body in a combustor that displayed velocity-coupled thermoacoustic instability. By using the complex network analysis, they could identify the wavemaker regions and modify the geometry near these regions to suppress the receptivity of the shear layer. The method relies on calculation of an undirected weighted spatial correlation network from the data; in this work, we use the velocity data as the input to the network. Each interrogation window of the velocity data is a node in the network and the strength of the connection between two nodes, i and j, is calculated using a Pearson correlation coefficient, Rij, as in Equation 2.

$$R_{ij} = \frac{\sum_{n=1}^{N} (u_{i}^{n} - \overline{u_{i}}) (u_{j}^{n} - \overline{u_{j}})}{\sqrt{\sum_{n=1}^{N} (u_{i}^{n} - \overline{u_{i}})^{2}} \sqrt{\sum_{n=1}^{N} (u_{j}^{n} - \overline{u_{j}})^{2}}}$$
(2)

In this definition, the velocity component of choice, u, is summed over the time index, n. Additionally, the number of samples, N, is 4000, and the bar over u indicates a time-average over the length of the data series. This correlation matrix is then used to calculate an adjacency matrix, A_{ij} , which defines the connectivity between nodes and is defined in Equation 3. Here, R_t is an adjacency threshold that is set to 0.5, although similar results are obtained at higher thresholds as well.

$$A_{ij} = \begin{cases} \left| R_{ij} \right|, & \left| R_{ij} \right| > R_t \& i \neq j \\ 0 & otherwise \end{cases}$$
(3)

Using this method, the adjacency matrix for two nodes, i and j, describes the magnitude of the correlation between velocity fluctuations at the two nodes and can be interpreted as the strength of the connection between these nodes. The final parameter that is calculated in this method is the weighted closeness centrality (WCC) of each node in the flow field, as defined in Equation 4,

$$C_i = \sum_{j=1, j \neq i}^{M} 2^{-d_{ij}}$$
 (4)

where d_{ij} is the least-costly path to traverse from location i to location j through locations h, k, ... r, s, that connect i and j, as in Equation 5.

$$d_{ij} = \min\left(\frac{1}{A_{ih}} + \frac{1}{A_{hk}} + \dots + \frac{1}{A_{rs}} + \frac{1}{A_{sj}}\right)$$
(5)

Dijkstra's algorithm [35] is used to calculate the minimization in Equation 5 over all possible paths between locations i and j as given by A_{ij} . In this analysis, we use this weighted closeness centrality parameter to interpret the data. The WCC has a high magnitude at a particular location when it is connected to a large number of other locations through low-cost paths, where the cost of the path is determined by how closely velocity oscillations between two connected locations are correlated. As such, the WCC provides a direct measure of how closely flow oscillations at a given location are correlated with oscillations at all other points in the flow. If a particular region has very high values of WCC, it is the result of strong coupling between the flow in that region and elsewhere, which is essentially the definition of a wavemaker region.

IV. Results

A. Test matrix

Seven different bluff-body configurations were used in this study: six cases with three bluff bodies and one case with a single bluff body, the latter being considered the single element "unit flow" to establish a baseline for the interacting cases and ensure our data is consistent with other experiments. For this investigation, the center-to-center spacing w was increased in 5 mm increments, a resolution that was deemed sufficient based off previous experimental investigations. Table 2 outlines the seven test cases along with their corresponding w/D values. The Reynolds number of the flow based on bluff-body diameter is 4,000; explanation of this choice of flow condition is discussed extensively in Meehan et al. [29].

Table 2. Test matrix with bluff-body spacings in mm.

Spacing [mm]	32	37	42	47	52	57	single wake
w/D	1.68	1.94	2.20	2.47	2.73	2.99	n/a

B. Time-averaged flow fields

The time-averaged flow profiles for the entire test matrix are shown in Figure 2. The flow profile of the single wake is representative of a standard wake profile. A recirculation zone is located downstream of the bluff body as a result of flow separation and the scale of the recirculation zone length is on the order of the bluff-body diameter. In the multiple-wake cases, recirculation zones are present downstream of each of the bluff bodies, although a bias in the flow direction is present in the multiple-wake cases as a result of the outer flow boundary conditions. The inward bias of the three-wake case was also noted by Sumner et al. [32].

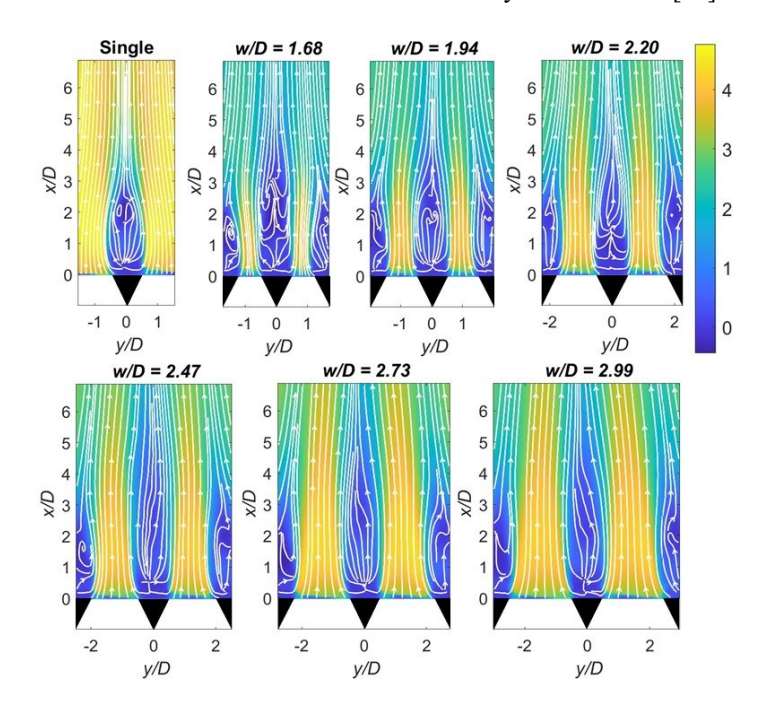


Figure 2. Time-averaged axial velocity with streamlines.

C. Single-wake analysis

The single-wake case provides a baseline for the multi-wake dynamics and also a platform for testing the utility of the new analysis tools on wake oscillations. Figure 3a shows the eigenvalue spectra obtained from the use of SPOD. As SPOD is an energy-based decomposition, the results are plotted with the most energetic mode (Mode 1) marked in red and the remaining modes descend in order of decreasing energy. The first mode peaks at 47 Hz, yielding a Strouhal number of St = 0.28. This Strouhal number is consistent with the that of the BVK instability. Furthermore, the energy of the peak of the first mode is much greater than the energy of the peaks in lower energy modes (note the logarithmic scale on the y-axis). The lower-energy modes do not contain any discernable peaks, and so only mode shapes from Mode 1 are analyzed.

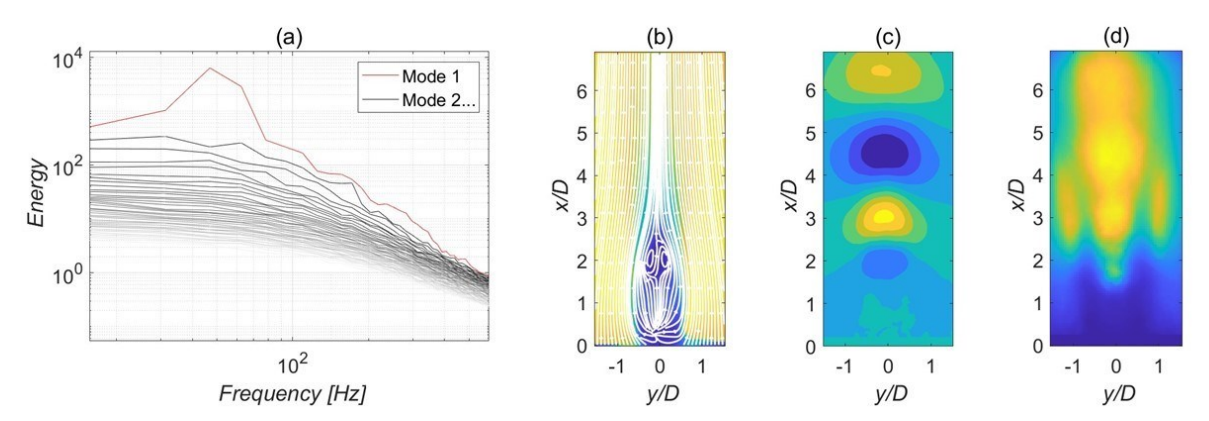


Figure 3. Results of the single-wake analysis, including a) SPOD modal energy spectrum, b) time-averaged flow field, c) mode shape of Mode 1 at 47 Hz from SPOD, and d) WCC from network analysis.

Figure 3c-d shows the time-averaged axial velocity, the transverse velocity mode shape of the first mode at 47 Hz obtained from SPOD, and the spatial distribution of the WCC. Recall that the WCC is a measure of the connectivity between the node and other parts of the region. As such, the value of the WCC is high in regions where the SPOD exhibits high amplitudes of oscillation as long as those oscillations are correlated in time and close in space to surrounding motions. The SPOD mode shape shows significant coherent oscillations with downstream distance in the wake, representative of the asymmetric vortex shedding of the BVK instability. The distribution of WCC reflects that of the SPOD mode shape. There are regions of high WCC that align with the regions of high oscillation amplitude in the SPOD mode shape at x/D=2, 3, 4.5, and 6.5. Additionally, there are two regions of high WCC on either side of the wake from about x/D=2-4. These are the shear layers, as can be seen in the velocity gradients at the edge of the wake structure in Figure 3b. The results of the WCC, when interpreted together with the SPOD, identify the source of the oscillation at the base of the recirculation zone ($x/D\approx1.5$) and the regions of high temporal coherence in the wake oscillation region. Further, it shows that the shear layer is oscillating in response to the wake oscillations. The strength of the shear layer oscillations is not as high as in the wake oscillations, as evidenced by the fact that they are missing from the Mode 1 in the SPOD.

Figure 4a shows the wavelet transform of the transverse velocity signal at the high-oscillation region at a downstream distance of approximately x/D = 3 for the single-wake case. Despite the strong peak in the SPOD eigenvalue spectrum, there is some temporal intermittency in the strength and frequency of vortex shedding at this location. This location is roughly one bluff body diameter away from the wave maker region, as exhibited in Figure 3b-c. Figure 4b shows the intermittency factor of the transverse velocity oscillations at each of the coherent regions in the SPOD mode as a function of downstream distance using a threshold of 50%. Initially, the intermittency factor is 0.6 near x/D = 2, which is a region that corresponds to the end of the recirculation zone, as indicated by the time-averaged axial velocity plotted on the same graph. An intermittency factor of 0.6 implies that the flow is coherent for 60% of the time, a value that increases with downstream distance. The intermittency factor value asymptotes towards 1 at x/D = 6.5.

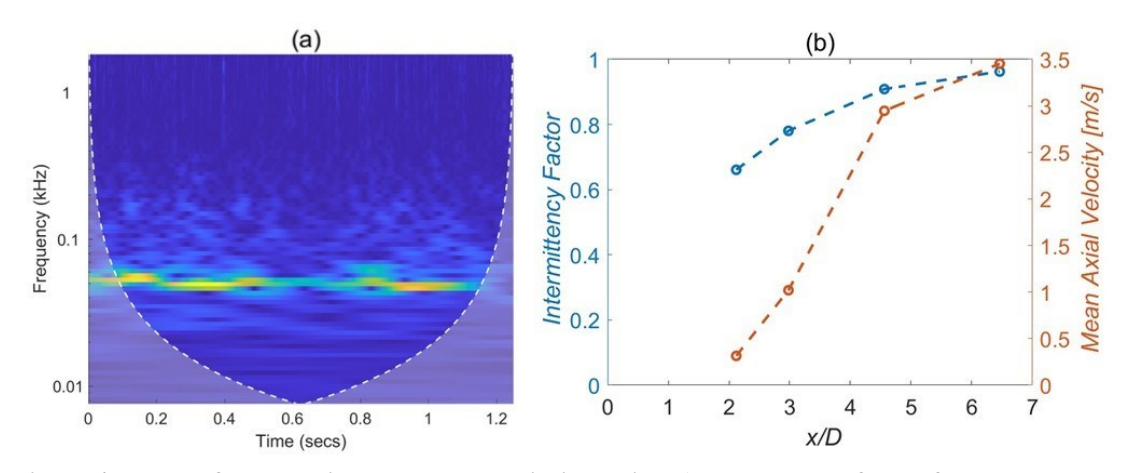


Figure 4. Results from the single-wake analysis, including a) wavelet transform of transverse velocity fluctuation at x/D = 3 and b) intermittency factor of oscillation as a function of downstream distance

D. Multiple-wake analysis

Figure 5 shows the energy spectra from SPOD for all the spacings of the three-wake configuration. With the addition of two more bluff bodies, the magnitude of the energy of the first mode decreases by an order of magnitude as compared to the single-wake case. In fact, the smallest spacing (Figure 5a) peaks at the lowest energy out of all the cases, including the single wake case. The peak energy increases as spacing increases, potentially indicating that the wakes begin to regain their "unit flow" behavior as the spacing increases and the level of interaction decreases. Additionally, the shape of the peak at the dominant shedding frequency is generally broader than that in the first mode of the single wake case; the lower energy modes are broader in shape as well. Spectral broadening in the peak is an indication of frequency jitter in the coherent oscillations in the flow field. In contrast to the single-wake case, many of the lower modes have spectrally-narrow content for several of the spacings, including Modes 2-4. As will be discussed next, these modes contain dynamically important flow features.

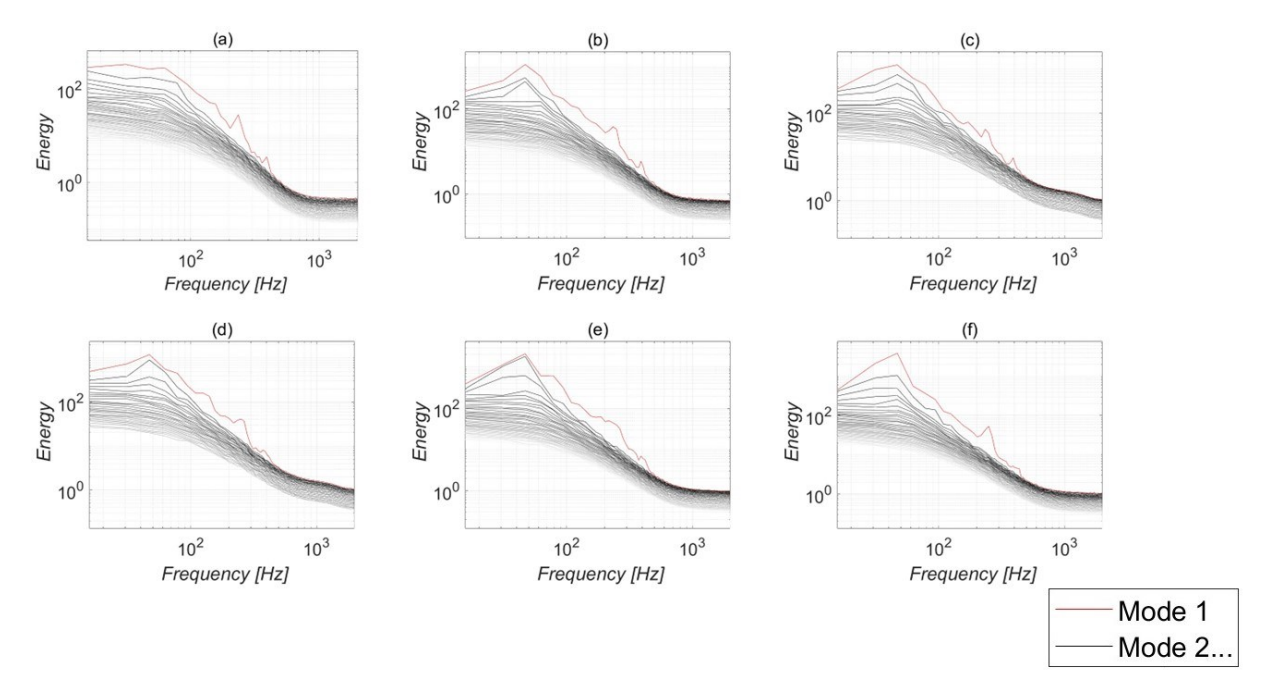


Figure 5. SPOD eigenvalue spectra for x/D = a) 1.68, b) 1.94, c) 2.20, d) 2.47, e) 2.73 f) 2.99

Figure 6 shows the transverse mode shapes from SPOD for Modes 1-3 at the peak shedding frequency for each of the multi-wake cases. In all cases except the closest spacing (w/D = 1.68), three distinct wakes are visible. The field of view is the same as in the time-averaged images in Error! Reference source not found., where only half of the outer two wakes is shown. For w/D = 1.68 (Figure 6a-c), the three wakes merge into one oscillating structure, as evidenced by large region of oscillation in the middle of the frame in Figure 6(a) and (b). The dynamics of individual wakes are much more evident at larger spacings. For the w/D = 1.94 spacing (Figure 6df), each mode predominantly contains the oscillations from one wake only; Mode 1 shows the left wake, Mode 2 the center wake, and Mode 3 the right wake. Based on the eigenvalue spectrum for this case in Figure 5(b), these are the only three modes with spectrally narrow content, and Mode 1 has a significantly higher amplitude than Modes 2 or 3. Figure 6g-I shows the mode shapes of the w/D = 2.20 case. This is the only spacing where oscillations from all three wakes appear in the first three modes, which according to Figure 5(c), are the only three modes with spectrally narrow content. In addition, w/D = 2.20 is the only case where the center wake oscillates in the first mode. For w/D = 2.47 and 2.73 (Figure 6j-1 and Figure 6m-0, respectively), the dominant structures in each wake are the same: the right wake for Mode 1, the left wake for Mode 2, and the center wake for Mode 3. In both these cases, Mode 1 and 2 have similar energies in the eigenvalue spectra (Figure 5d-e), whereas Mode 3 is significantly weaker. At the largest spacing, w/D = 2.99 (Figure 6p-r), two wakes are present in each mode: the left and the right wake. They oscillate strongly and oscillate out of phase in Mode 1. This corresponds to a strong peak in the first mode energy in the eigenvalue spectra (Figure 5f).

Table 3 organizes the dominant wake structures for each spacing for the first three modes; the closest spacing is not included in the table as the dynamics of the three wakes are not separable. The first wake of interest in these cases is the center wake. Apart from w/D = 2.20, where all three wakes appear in all three modes, the center wake does not appear the first mode. In these cases, the center wake appears only once in Mode 2 for w/D = 1.94 and 2.99 and in Mode 3 for w/D = 2.47 and 2.73. Oscillations in the right and left wakes are generally stronger than that of the center wake, although neither wake is dominant across the entire w/D parameter space.

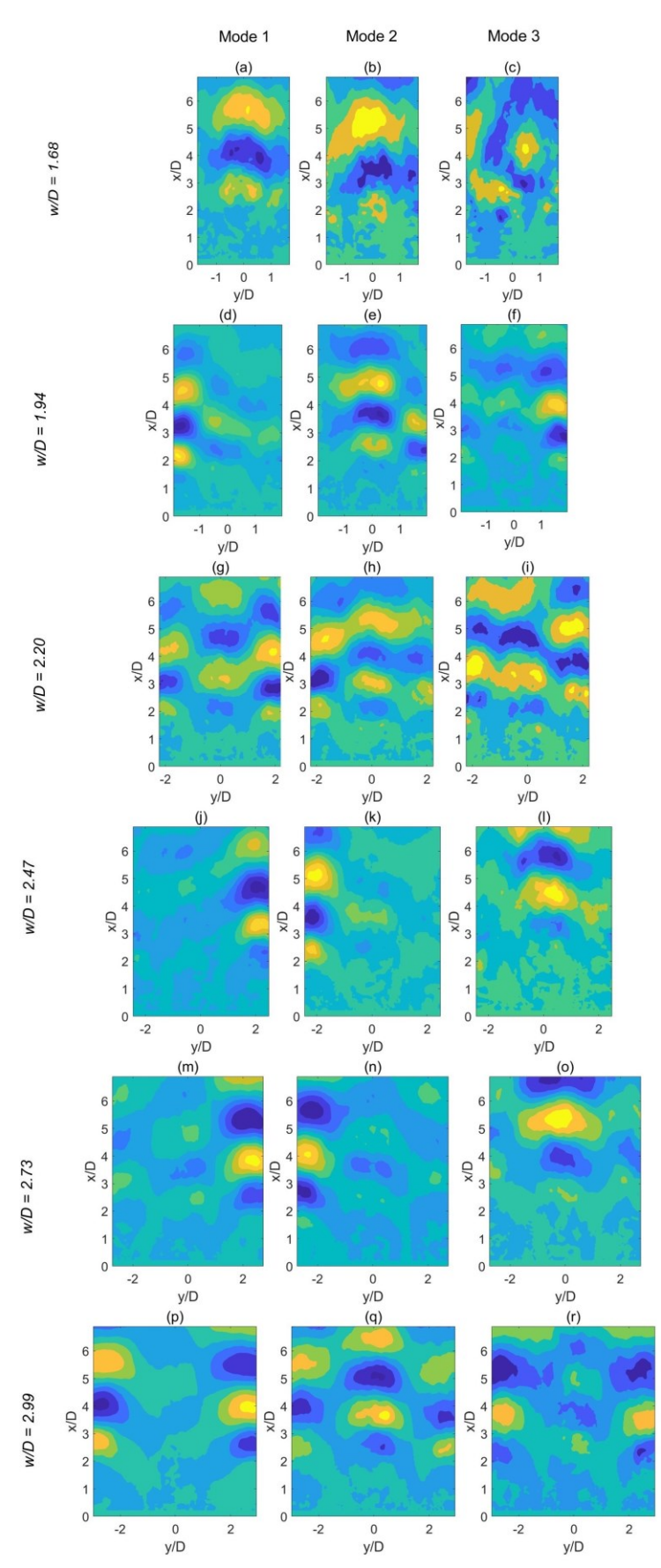


Figure 6. SPOD modes 1-3 at the peak frequency of 47 Hz for (a-c) x/D = 1.68, (d-f) x/D = 1.94, (g-i) x/D = 2.20, (j-l) x/D = 2.47, (m-o) x/D = 2.73, (p-r) x/D = 2.99.

Table 3. Dominant wake structures in each mode.

w/D	Mode 1	Mode 2	Mode 3
1.94	Left	Center	Right
2.20	Left, Right, Center	Left, Right, Center	Left, Right, Center
2.47	Right	Left	Center
2.73	Right	Left	Center
2.99	Left, Right	Left, Right, Center	Left, Right

There are two reasons why the energy of a particular oscillation, like the center wake, could be lower in a SPOD analysis. The first reason is that the oscillation is continuous but of lower amplitude. The second reason is that the oscillation is more intermittent, such that oscillation occurs over a shorter total time in the time series. To understand both these effects, the *IF* (Figure 7a) and the RMS velocity (Figure 7b) is plotted as a function of wake spacing for all three wakes; the RMS and *IF* are calculated at the second downstream region of high-intensity oscillation from the SPOD modes shown in Figure 6, generally located near x/D = 3. Here, the single wake is plotted as a center wake at w/D = 0 as a point of comparison. Additionally, only the center wake was plotted for w/D = 1.68 because of the difficulty in distinguishing the left and the right wakes in the SPOD modes.

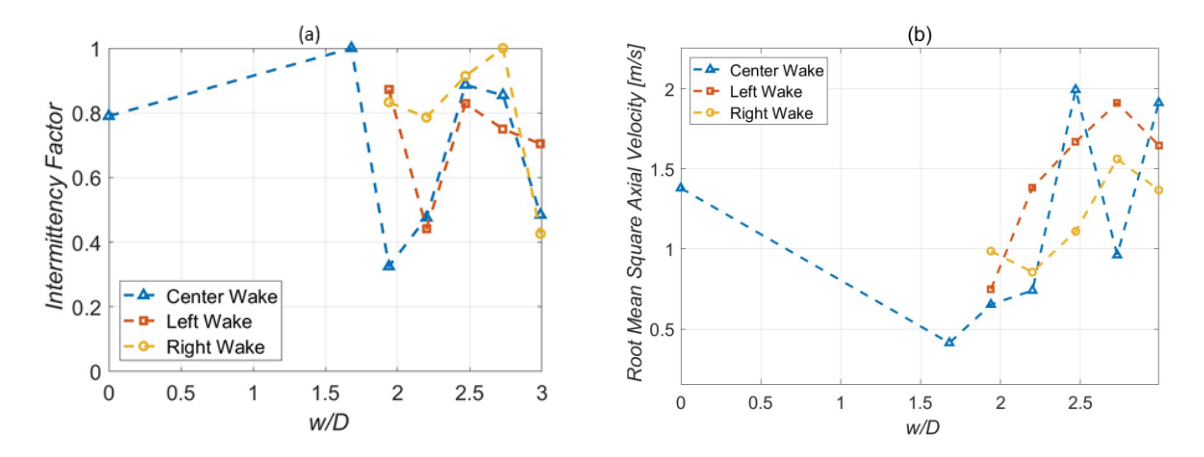


Figure 7. a) *IF* and b) RMS velocity for the center, left, and right wakes as a function of bluff body spacing *w/D* for the second region of oscillation.

The *IF* of the center wake is relatively high for both the single-wake case and the w/D = 1.68 case, where the three wakes are merged into one structure. At larger spacings, the behavior of the center wake is highly variable and non-monotonic in terms of both *IF* and RMS. In general, the right wake has a high *IF* relative to the other wakes. The RMS of the left and right wake generally increase with increasing spacing until the final spacing, where the RMS levels decrease slightly. The *IF* and RMS velocity oscillations of each wake do not always align with the mode strength found in SPOD, detailed in Table 3, where the RMS and *IF* somewhat align, on net, with the modal ordering for w/D = 2.20, 2.73, and 2.99, but do not for w/D = 1.94 and 2.47. For example, the intermittency factor of the center wake drops sharply to less than 0.4 and the RMS increases by a smaller margin at w/D = 1.94, the spacing where the center wake oscillation only appears in the second mode. At this same spacing, the *IF*s are significantly higher for the right and left wakes than the center wake, but the RMS velocity oscillations are of similar magnitudes. As a result, one would expect the center mode to have a less dynamically significant role than the SPOD ordering suggestions. In contrast, the *IF* and RMS results for w/D = 2.73 align more closely with the SPOD modal results. Here, the RMS velocities in the right and left wakes are higher than the center wake, whereas the *IF* are similar. The ordering of the SPOD modes aligns with these results.

One of the reasons for the disagreement may be a result of the filtering operation in the calculation of IF from the wavelet transform. Figure 8 shows the spectrograms obtained from the wavelet transforms for the left, center, and right wakes for the w/D = 2.73 case. As seen in Figure 8a, the velocity signal from the probe in the left wake experiences bursts of high magnitude frequency content throughout the signal. Figure 7b shows that the RMS velocity is the highest for the left wake throughout all the spacings and is also greater than the RMS velocity of the right and center wakes. The IF for the wake at this point is below 0.8, so the signal spends more time coherent than it does incoherent. In the right wake (Figure 8c), the spectrogram has similar amplitudes of oscillation as the left wake when the right wake is oscillation, although contains fewer periods of strong oscillation than the left wake. The RMS of this wake oscillation is lower than that of the left wake as a result. However, the intermittency factor for this wake is 1, meaning that the signal is coherent the entire time given the threshold applied in this

case. Finally, the center wake (Figure 8b) shows lower magnitude content for a greater range of frequencies over the time signal. As a result, the RMS has dropped for this wake at this spacing and the intermittency factor implies that the oscillation is relatively continuous (Figure 7a). The spectrogram shows that the center wake is more subject to phase jitter, or fluctuations in frequency, than the left or the right wake. This phase jitter results in oscillations at a broader range of frequencies, driving the increase in *IF*. These results show the sensitivity of the results to choices in frequency bandwidth and threshold in the calculation of *IF*, but also highlight the complex dynamics present in the center wake. This wake experiences higher levels of interaction with the adjacent wakes, driving more variable behavior in both amplitude and frequency space as spacing between the wakes varies.

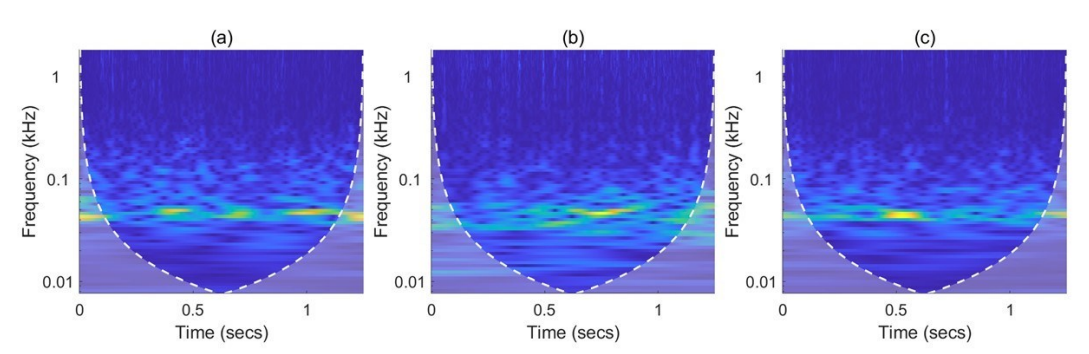


Figure 8. Spectrogram resulting from the wavelet transform for the a) left, b) center, and c) right wake.

The final analysis performed in this study was the calculation of the WCC parameter. Figure 9 shows the WCC parameter together with the time-averaged flow structure and the mode shape for Mode 1 at the peak frequency from the SPOD analysis for each of the spacings. The time-averaged flow and Mode 1 shapes are repeated in this figure to provide context for the regions of high WCC at each of the spacings. In general, the maximum value of the WCC increases with increasing bluff body spacing. Furthermore, the regions with the greatest area values of WCC (seen in Figure 9f, l, o, and r) are those that mirror the shape of Mode 1 (seen in Figure 9e, k, n, and q). The WCC also displays measurable values in the regions that mirror the shape of Mode 2 and Mode 3, although not as high as those in Mode 1. This similarity between the WCC and Mode 1 shape is indicative of the high level of correlation between motions in the region with the highest amplitude coherent motion.

At the smallest spacing (w/D = 1.68, Figure 9a-c), significant magnitude of WCC is found in several regions of the flow, including far downstream of the bluff bodies (x/D > 5), in the left and right wakes, and, most interestingly, in the separation regions of the shear layers at the trailing edge of the bluff body. The shear layers near the bluff also are highly connected to other regions of the flow, according to Figure 9c, a phenomenon that decreases in strength with increasing bluff body spacing. This finding is important, as it demonstrates the relative dominance between the shear layer vs. wake instability in the flow at different spacings. In spacings where the wakes do not interact as strongly, or in the single-wake case where there is no interaction at all, the wake mode is able to dominate the level of coherent, connected motion. However, the high level of interaction at the closest spacing disrupts the structure of the interact wakes and the shear layer instability amplitude is measurable. Some level of WCC in the shear layer separation point is present in all multi-wake cases, although at varying magnitudes, indicating the complexity of the interaction of the wake modes and possible interaction of the shear layer modes. This same feature is completely missing from the single-wake case, indicating a change in the shear layer dynamics in the presence of flow interaction.

Increasing the bluff body spacing to w/D = 1.94 (Figure 9d-f) decreases the magnitude of the shear layer activity with respect to the rest of the flow field. The region with the highest value of WCC corresponds to the left wake oscillation, also seen in Mode 1. The center and right wakes oscillate strongly in the second and third mode, with weaker values of WCC in the corresponding regions of the flow. Similar to w/D = 1.68, w/D = 2.20(Figure 9g-i) has a large value of WCC along the centerline near x/D = 4. The SPOD plot shows that this region corresponds with the region of center wake oscillation. The left and the right wakes are present in Mode 1 of the SPOD as well, although the strength of the WCC is weaker in those regions. The results at w/D = 2.47 (Figure 9j-1) show only one wake oscillation in each of the first three SPOD modes. In the WCC plot (Figure 9j), the regions of high WCC correspond to oscillations in the right and left wakes for the first and second mode of SPOD, respectively. The center wake, according to Figure 9j, has a higher value of WCC that biases towards the right wake. This finding is indicative that the WCC may identify dynamics that are not depicted in the high-energy modes of SPOD but are still highly connected to other regions of the flow. Increasing the bluff body spacing to w/D = 2.73 (Figure 9m-o) results in a similar WCC result as that from the w/D = 2.47 case, with a stronger WCC in the right wake (present in Mode 1) and weaker WCC in the left wake (present in Mode 1). In the final spacing, w/D = 2.99, the left and the right wakes look like two single wake cases in both the SPOD and WCC analyses. In addition to one large area of high WCC downstream of the left and right bluff bodies, these regions also have a long and thin region of large WCC corresponding to the shear layers.

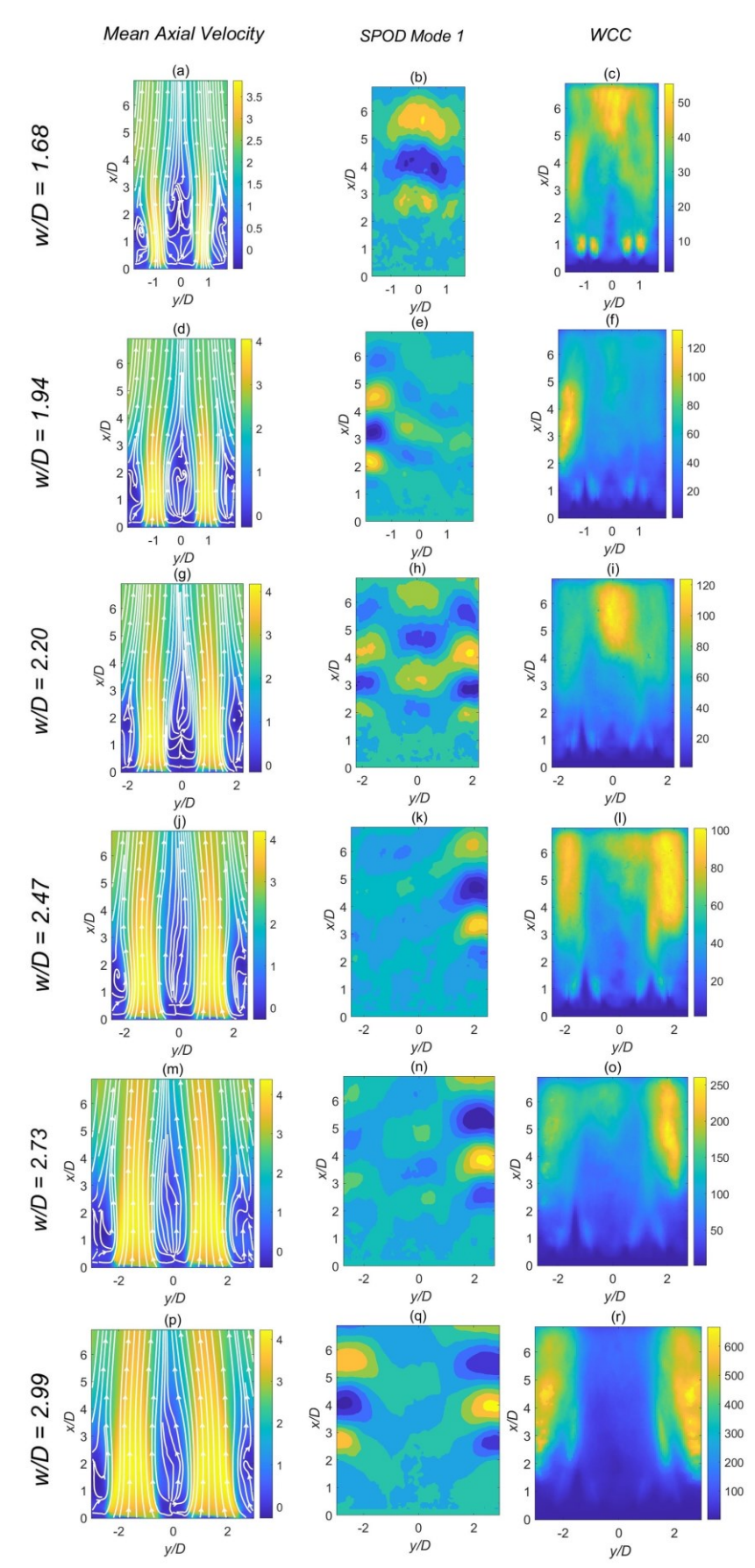


Figure 9. Time-averaged velocity, SPOD Mode 1, WCC (left to right) for (a-c) w/D = 1.68, (d-f) w/D = 1.94, (g-i) w/D = 2.20, (j-l) w/D = 2.47, (m-o) w/D = 2.73, (p-r) w/D = 2.99.

V. Conclusions

The present work considers the dynamics of a three-wake system using a combination of analysis tools – wavelet transforms, spectral proper orthogonal decomposition, and complex network analysis – to understand the temporal and modal dynamics of this complex flow field. When applied to a single-wake flow, the tools provided additional insight into a canonical flow behavior. The SPOD identified the BVK wake-shedding mode at a frequency of 47 Hz or a Strouhal number of St = 0.28, which is within the predicted range from linear stability theory. The wavelet analysis showed that the wake shedding displayed some intermittency in time, where the IF was used to quantify this behavior. Sensitivity of the IF to choices of filter bandwidth and threshold were discussed. The complex network analysis was used to calculate the weighted closeness centrality, which is a measure of the coherence and connectedness of an oscillation in one point of the flow to all other points. The WCC was high in the wavemaker region and the region of wake oscillation downstream.

The multi-wake case displayed highly intermittent dynamics. The closest spacing tested, w/D = 1.68, showed significant merging of the three wakes and SPOD identified one merged structure of oscillation without a strong peak in the eigenvalue spectrum. At larger spacings, the three wakes were not merged and displayed highly intermittent dynamics, with the central wake showing the highest level of variability in its dynamics as the spacing was varied. SPOD identified the shedding of individual wakes in various modes, all near 47 Hz, indicating a variation in the energy content of the shedding between the three wakes. This mode ranking was compared to both the IF and the RMS of the velocity oscillation in the wake, showing the sensitivity of the result to the calculation of IF. Finally, the WCC showed strong oscillations in the shear layer separation region for the closest spacing, whereas the shear layer region had a lower WCC for the wider spacing cases. In all three-wake cases, however, the WCC parameter showed a distinction pattern in the shear layer separation region, whereas it was completely absent in the single-wake case. This difference in the shear layer coherence and connectedness to the other oscillations in the flow field will be investigated in future work. The result suggests a potentially more dynamically important role of the shear layer as compared to the wake in the interacting-wake flow as compared to a single-wake flow. Finally, the WCC magnitude was strong in the regions where wake shedding was strong as indicated with Mode 1 of the SPOD analysis.

The results of this study suggest that there is significant interaction between wakes in multi-wake systems and that both the shear layer and downstream wake-shedding region play important dynamical roles in this interaction. Future work will make future use of these analysis tools to understand the dynamical significance and potential causal relationship between oscillations in different parts of this complex flow.

Acknowledgments

This work is supported by the National Science Foundation with grant CBET-1749679. Any opinions, findings, and conclusions or recommendations expressed in this material are those of the authors and do not necessarily reflect the views of the National Science Foundation. The authors would like to thank Ashwini Karmarkar for support on the analysis and Dr. Ankit Tyagi for support on the data acquisition.

References

- [1] Lieuwen, T. C. *Unsteady Combustor Physics*. Cambridge University Press, 2012.
- [2] Alam, M. M., Zhou, Y., and Wang, X. W. "The wake of two side-by-side square cylinders." *Journal of Fluid Mechanics*, Vol. 669, 2011, pp. 432–471. https://doi.org/10.1017/S0022112010005288.
- [3] Zhou, Y., and Alam, M. M. "Wake of two interacting circular cylinders: A review." *International Journal of Heat and Fluid Flow*, Vol. 62, 2016, pp. 510-537 https://doi.org/10.1016/j.ijheatfluidflow.2016.08.008.
- [4] Schewe, G. "Reynolds-number effects in flow around more-or-less bluff bodies." *Journal of Wind Engineering and Industrial Aerodynamics*, Vol. 89, Nos. 14–15, 2001, pp. 1267–1289. https://doi.org/10.1016/S0167-6105(01)00158-1.
- [5] Derakhshandeh, J. F., and Alam, M. M. "A review of bluff body wakes." *Ocean Engineering*, Vol. 182, 2019, pp. 475–488. https://doi.org/10.1016/j.oceaneng.2019.04.093.
- [6] Feshalami, B. F., He, S., Scarano, F., Gan, L., and Morton, C. "A review of experiments on stationary bluff body wakes." *Physics of Fluids*, Vol. 34, 2022, pp. 11301. https://doi.org/10.1063/5.0077323.
- [7] Shanbhogue, S. J., Husain, S., and Lieuwen, T. "Lean blowoff of bluff body stabilized flames: Scaling and dynamics." *Progress in Energy and Combustion Science*, Vol. 35, No. 1, 2009, pp. 98-120. https://doi.org/https://doi.org/10.1016/j.pecs.2008.07.003.
- [8] Williamson, C. H. K. "Vortex dynamics in the cylinder wake." *Annual Review of Fluid Mechanics*, Vol. 28, 1996, pp. 477-539. https://doi.org/10.1146/annurev.fl.28.010196.002401.
- [9] Huerre, P., and Monkewitz, P. A. "Absolute and convective instabilities in free shear layers." *Journal of Fluid Mechanics*, Vol. 159, 1985, pp. 151-168. https://doi.org/10.1017/S0022112085003147.
- [10] Brown, G., and Roshko, A. "On density effects and large structure in turbulent mixing layers." *Journal of Fluid Mechanics*, Vol. 64, No. 4, 1974, pp. 775–816. https://doi.org/10.1017/S002211207400190X.

- [11] Jeong, J., and Hussain, F. "On the identification of a vortex." *Journal of Fluid Mechanics*, Vol. 285, 1995, pp. 69–94. https://doi.org/10.1017/S0022112095000462.
- [12] Hussain, A. K. M. F. "Coherent structures reality and myth." *Physics of Fluids*, Vol. 26, No. 10, 1983. pp. 2816. https://doi.org/10.1063/1.864048.
- [13] Pier, B. "Local and global instabilities in the wake of a sphere." *Journal of Fluid Mechanics*, Vol. 603, 2008, pp. 39–61. https://doi.org/10.1017/S0022112008000736.
- [14] Chomaz, J. M. "Global instabilities in spatially developing flows: Non-normality and nonlinearity." *Annual Review of Fluid Mechanics*, Vol. 37, 2005, pp. 357–392. https://doi.org/10.1146/annurev.fluid.37.061903.175810.
- [15] Juniper, M. P. "The effect of confinement on the stability of non-swirling round jet/wake flows." *Journal of Fluid Mechanics*, Vol. 605, 2008, pp. 227–252. https://doi.org/10.1017/S0022112008001547.
- [16] Chomaz, J. M., Huerre, P., and Redekopp, L. G. "A frequency selection criterion in spatially developing flows." *Studies in Applied Mathematics*, Vol. 84, 1991, pp. 119–144. https://doi.org/10.1002/sapm1991842119.
- [17] Monkewitz, P. A., Huerre, P., and Chomaz, J. M. "Global linear stability analysis of weakly non-parallel shear flows." *Journal of Fluid Mechanics*, Vol. 251, 1993, pp. 1–20. https://doi.org/10.1017/S0022112093003313.
- [18] Rees, S. J., and Juniper, M. P. "The effect of confinement on the stability of viscous planar jets and wakes." *Journal of Fluid Mechanics*, Vol. 656, 2010, pp. 309–336. https://doi.org/10.1017/S0022112010001060.
- [19] Yu, M. H., and Monkewitz, P. A. "The effect of nonuniform density on the absolute instability of two-dimensional inertial jets and wakes." *Physics of Fluids A*, Vol. 2, No. 7, 1990, pp. 1175–1181. https://doi.org/10.1063/1.857618.
- [20] Juniper, M. P. "The effect of confinement on the stability of two-dimensional shear flows." *Journal of Fluid Mechanics*, Vol. 565, 2006, pp. 171–195. https://doi.org/10.1017/S0022112006001558.
- [21] Juniper, M. P. "The full impulse response of two-dimensional jet/wake flows and implications for confinement." *Journal of Fluid Mechanics*, Vol. 590, 2007, pp. 163–185. https://doi.org/10.1017/S0022112007007975.
- Juniper, M. P., Tammisola, O., and Lundell, F. "The local and global stability of confined planar wakes at intermediate Reynolds number." *Journal of Fluid Mechanics*, Vol. 686, 2011, p. 218. https://doi.org/10.1017/jfm.2011.324.
- [23] Perry, A. E., Chong, M. S., and Lim, T. T. "The vortex-shedding process behind two-dimensional bluff bodies." *Journal of Fluid Mechanics*, Vol. 116, 1982, pp. 77-90. https://doi.org/10.1017/S0022112082000378.
- [24] Prasad, A., and Williamson, C. H. K. "The instability of the shear layer separating from a bluff body." *Journal of Fluid Mechanics*, Vol. 333, 1997, pp. 375 402. https://doi.org/10.1017/S0022112096004326.
- [25] Shanbhogue, S., Shin, D. H., Hemchandra, S., Plaks, D., and Lieuwen, T. "Flame sheet dynamics of bluff-body stabilized flames during longitudinal acoustic forcing." *Proceedings of the Combustion Institute*, Vol. 32 II, 2009, pp. 1787–1794. https://doi.org/10.1016/J.PROCI.2008.06.034.
- [26] Emerson, B., O'Connor, J., Juniper, M., and Lieuwen, T. "Density ratio effects on reacting bluff-body flow field characteristics." *Journal of Fluid Mechanics*, Vol. 706, 2012, p. 219. https://doi.org/10.1017/jfm.2012.248.
- [27] Ko, N. W. M., and Lau, K. K. "Flow structures in initial region of two interacting parallel plane jets." *Experimental Thermal and Fluid Science*, Vol. 2, No. 4, 1989, pp. 431–449. https://doi.org/10.1016/0894-1777(89)90006-X.
- [28] Sebastian, J., Emerson, B., and O'Connor, J. "Spatio-temporal stability analysis of linear arrays of 2D density stratified wakes and jets." *Physics of Fluids*, Vol. 30, 2018, p. 114103. https://doi.org/10.1063/1.5053773.
- [29] Meehan, M., Tyagi, A., and O'Connor, J. "Flow Dynamics in a variable-spacing, three bluff-body flowfield." *Physics of Fluids*, Vol. 30, No. 2, 2018, pp. 025105. https://doi.org/10.1063/1.5001943.
- [30] Wang, Z. J., and Zhou, Y. "Vortex interactions in a two side-by-side cylinder near-wake." *International Journal of Heat and Fluid Flow*, Vol. 26, No. 3, 2005, pp. 362–377. https://doi.org/10.1016/J.IJHEATFLUIDFLOW.2004.10.006.
- [31] Carini, M., Giannetti, F., and Auteri, F. "On the origin of the flip-flop instability of two side-by-side cylinder wakes." *Journal of Fluid Mechanics*, Vol. 742, 2014, pp. 552–576. https://doi.org/10.1017/jfm.2014.9.
- [32] Sumner, D., Wong, S. S. T., Price, S. J., and Païdoussis, M. P. "Fluid behavior of side-by-side circular cylinders in steady cross-flow." *Journal of Fluids and Structures*, Vol. 13, No. 3, 1999, pp. 309-338. https://doi.org/10.1006/jfls.1999.0205.

- [33] Zheng, Q., and Alam, M. M. "Intrinsic features of flow past three square prisms in side-by-side arrangement." *Journal of Fluid Mechanics*, Vol. 826, 2017, pp. 996-1033. https://doi.org/10.1017/jfm.2017.378.
- [34] Dare, T. P., Berger, Z. P., Meehan, M., and O'Connor, J. "Cluster-based reduced-order modeling to capture intermittent dynamics of interacting wakes." *AIAA Journal*, Vol. 57, No. 7, 2019, pp. 2819–2827. https://doi.org/10.2514/1.J057623.
- [35] Towne, A., Schmidt, O. T., and Colonius, T. "Spectral proper orthogonal decomposition and its relationship to dynamic mode decomposition and resolvent analysis." *Journal of Fluid Mechanics*, Vol. 847, 2018, pp. 821–867. https://doi.org/10.1017/jfm.2018.283.
- [36] Yin, Z., and Stöhr, M. "Time-frequency localisation of intermittent dynamics in a bistable turbulent swirl flame." *Journal of Fluid Mechanics*, Vol. 882, 2020, pp. A30. https://doi.org/10.1017/jfm.2019.762.
- [37] Karmarkar, A., Tyagi, A., Hemchandra, S., and O'Connor, J. "Impact of turbulence on the coherent flame dynamics in a bluff-body stabilized flame." *Proceedings of the Combustion Institute*, Vol. 38, No. 2, 2021, pp. 3067-3075. https://doi.org/10.1016/j.proci.2020.08.059.
- [38] Hashimoto, T., Shibuya, H., Gotoda, H., Ohmichi, Y., and Matsuyama, S. "Spatiotemporal dynamics and early detection of thermoacoustic combustion instability in a model rocket combustor." *Physical Review E*, Vol. 99, No. 3, 2019, p. 032208. https://doi.org/10.1103/PhysRevE.99.032208.
- [39] Kasthuri, P., Krishnan, A., and Gejji, R. "Investigation into the coherence of flame intensity oscillations in a model multi-element rocket combustor using complex networks." *Physics of Fluids*, Vol. 34, 2022, p. 34107. https://doi.org/10.1063/5.0080874.
- [40] Krishnan, A., Manikandan, R., Midhun, P. R., Reeja, K. v., Unni, V. R., Sujith, R. I., Marwan, N., and Kurths, J. "Mitigation of oscillatory instability in turbulent reactive flows: A novel approach using complex networks." *EPL*, Vol. 128, No. 1, 2019, pp. 14003. https://doi.org/10.1209/0295-5075/128/14003.
- [41] Karmarkar, A., Gupta, S., Boxx, I., Hemchandra, S., and O'Connor, J. "Impact of precessing vortex core dynamics on the thermoacoustic instabilities in a swirl-stabilized combustor." *Journal of Fluid Mechanics*, Vol. 946, 2022, p. A36. https://doi.org/10.1017/jfm.2022.610.